Journal of the Korean Nuclear Society
Volume 36, Number 2, pp.153 ~ 164, April, 2004

Numerical Analysis of the Turbulent Flow and Heat Transfer in a Heated Rod Bundle

Wang-Kee In, Chang-Hwan Shin, Dong-Seok Oh, and Tae-Hyun Chun
Korea Atomic Energy Research Institute
150 Deokjin-dong, Yuseong-gu, Daejeon, 305-353, Korea
wkin@kaeri.re.kr

(Received October 30, 2003)

Abstract

A computational fluid dynamics (CFD) analysis has been performed to investigate the turbulent flow and heat transfer in a triangular rod bundle with pitch-to-diameter ratios (P/D) of 1.06 and 1.12. Anisotropic turbulence models predicted the turbulence-driven secondary flow in a triangular subchannel and the distributions of the time mean velocity and temperature, showing a significantly improved agreement with the measurements from the linear standard k-ε model. The anisotropic turbulence models predicted the turbulence structure for a rod bundle with a large P/D fairly well, but could not predict the very high turbulent intensity of the azimuthal velocity observed in the narrow flow region (gap) for a rod bundle with a small P/D.

Key Words : rod bundle, CFD, turbulence, heat transfer, secondary flow

1. Introduction

Most reactor fuel elements generally consist of rod bundles with coolant flowing axially through subchannels formed between the rods. The fuel rods are arranged in either square or equilateral triangular pitched arrays. An understanding of the detailed structure of the turbulent flow in the rod bundle, used especially as nuclear fuel elements, is of major interest to the nuclear power industry for safe and reliable plant operation. There have been many experiments performed on an axially developed turbulent flow in a bare rod bundle. Carajilescov and Todreas[1] provided an experimental and analytical study of an axial turbulent flow in a triangular rod bundle and Vonka[2] measured the secondary flow in an interior subchannel of a triangular rod bundle. Numerous experiments have been comducted on an axial turbulent flow in a square rod bundle[3-6]. Rehme[6] reviewed the main features of the turbulence structure in the subchannels of bare rod bundles as a secondary flow due to turbulence anisotropy and macroscopic flow pulsation due to a large eddy motion. Krauss and Meyer[7] presented experimental results on the turbulent transport of momentum and energy in a central channel of 37-rod heated bundles with a triangular array.

Few computational studies have been performed on turbulent flow in a red bundle since accurate

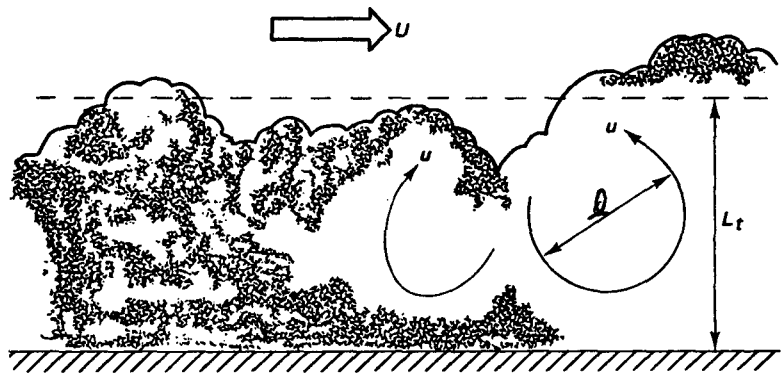

Fig. 1. Large Eddies in a Turbulent Boundary Layer. The Eddies Have Velocities *u* and the Largest Eddy Size (*l*) is Comparable to the Boundary-layer Thickness (L_t)

prediction is difficult due to the complexity of the turbulence phenomena. Slagter[8] published the finite element solution of a bare rod bundle flow using a one-equation turbulence model. Lee and Jang[9] and Lemos and Asato[10] provided numerical simulations of the triangular rod bundle flow using nonlinear eddy viscosity models. In et al.[11, 12] investigated the prediction performance of anisotropic turbulence models for a turbulent rod-bundle flow using a CFD code. They compared the predictions of the nonlinear quadratic k-ε models(Speziale[13], Shih et al.[14]) and cubic k-ε model(Craft et al.[15]), and the differential Reynolds stress models(RSM) by Launder-Reece-Rodi(LRR)[16] against those of the linear k-ε model(Launder and Spalding[17]). They reported that the nonlinear quadratic model by Speziale and the RSM by LRR showed significant improvements over the other turbulence models. A numerical simulation of the turbulent flow structure in the rod bundles is still required to evaluate the adequacy of the numerical work.

The objective of this paper is to compare the CFD predictions of the turbulent heat transfer in a rod bundle using various turbulence models. The turbulence models used in this study are the linear k-ε model, the nonlinear quadratic k-ε model by Speziale and the Reynolds stress models by LRR and Speziale-Sarkar-Gatski(SSG)[18].

2. Turbulence Model

Most flows occurring in nature and in engineering applications are turbulent. Turbulent flow is an eddying motion that exists at high Reynolds numbers. Turbulence has a wide spectrum of eddy sizes with a corresponding spectrum of fluctuation frequencies. Turbulence has a prevailing rotational motion that can be thought of as a tangle of vortex elements with highly unsteady vorticity vectors that are aligned in all directions (Figure 1). The large eddies have sizes on the same order of magnitude as the flow domain, have low frequencies, and are a affected by the boundaries and the mean flow. The smallest eddies, on the other hand, are determined by the viscosity of the fluid and have high frequency fluctuations. Since turbulence consists of random fluctuations of the various flow properties, we use a statistical approach in which all quantities are expressed as the sum of mean and fluctuating parts. The time average of the continuity and Navier-Stokes equations leads to the Reynolds averaged Navier-Stokes(RANS) equations. The RANS equations include an additional set of terms, the Reynolds stresses, which have to be accurately

represented in terms of known quantities. Turbulence modeling is required to achieve closure of the Reynolds stresses by supplementary transport equations. The closure models range from the eddy viscosity model to the full second-order closure models, which represent each component of the Reynolds stress tensor on the mean flow.

The linear standard k-ε model of Launder and Spalding[17] uses an eddy viscosity hypothesis for the turbulence which states that the Reynolds stresses can be linearly related to the mean velocity gradients in a manner analogous to the relationship between the stress and strain tensor in a laminar Newtonian flow. The transport equations for the turbulent kinetic energy k and its dissipation rate ε are

$$\rho\frac{\partial k}{\partial t}+\rho U_j\frac{\partial k}{\partial x_j}=\tau_{ij}\frac{\partial U_i}{\partial x_j}-\rho\varepsilon+\frac{\partial}{\partial x_j}\left[\left(\mu+\mu_t/\sigma_k\right)\frac{\partial k}{\partial x_j}\right], \quad (1)$$

and

$$\rho\frac{\partial \varepsilon}{\partial t}+\rho U_j\frac{\partial \varepsilon}{\partial x_j}=C_{\varepsilon 1}\frac{\varepsilon}{k}\tau_{ij}\frac{\partial U_i}{\partial x_j}-C_{\varepsilon 2}\rho\frac{\varepsilon^2}{k}+\frac{\partial}{\partial x_j}\left[\left(\mu+\mu_t/\sigma_\varepsilon\right)\frac{\partial \varepsilon}{\partial x_j}\right], \quad (2)$$

where the Reynolds stress tensor τ_{ij} and eddy viscosity μ_t are defined as

$$\tau_{ij}=-\rho\overline{u_i'u_j'}=\mu_t\left(\frac{\partial U_i}{\partial x_j}+\frac{\partial U_j}{\partial x_i}\right)-\frac{2}{3}\rho k\delta_{ij} \quad (3)$$

$$\mu_t=\rho C_\mu\frac{k^2}{\varepsilon}. \quad (4)$$

The closure coefficients for the standard k-ε model are as follows:

$$C_\mu=0.09, C_{\varepsilon 1}=1.44, C_{\varepsilon 2}=1.92, \sigma_k=1.0, \sigma_\varepsilon=1.3. \quad (5)$$

The sum of the two terms on the left-hand side of Eq. (1) indicates the unsteady term and the convection of k. The first term on the right-hand side is known as production and represents the rate at which kinetic energy is transferred from the mean flow to the turbulence. The second term, known as dissipation, is the rate at which turbulence kinetic energy is converted into thermal internal energy. The last term is the sum of molecular and turbulent diffusion, representing the diffusion of turbulence energy caused by the natural molecular transport and turbulent fluctuations. Similarly, the three terms on the right-hand side of Eq. (2) are generally regarded as production of dissipation, dissipation of dissipation, and the sum of molecular diffusion of dissipation and turbulent transport of dissipation.

In order to mitigote the weakness of the isotropic eddy viscosity assumption used in the standard k-ε model, a nonlinear quadratic relationship for the Reynolds stresses was proposed as follows:

$$\begin{aligned}\rho\overline{u_i'u_j'}=&-\mu_t S_{ij}+\frac{2}{3}\rho k\delta_{ij}+C_1\mu_t\frac{k}{\varepsilon}\left(S_{ik}S_{kj}-\frac{1}{3}S_{kl}S_{kl}\delta_{ij}\right)\\&+C_2\mu_t\frac{k}{\varepsilon}\left(\Omega_{ik}S_{kj}+\Omega_{jk}S_{ki}\right)\\&+C_3\mu_t\frac{k}{\varepsilon}\left(\Omega_{ik}\Omega_{jk}-\frac{1}{3}\Omega_{ik}\Omega_{jk}\delta_{ij}\right)\end{aligned} \quad (6)$$

where

$$S_{ij}=\left(\frac{\partial U_i}{\partial x_j}+\frac{\partial U_j}{\partial x_i}\right),\quad \Omega_{ij}=\left(\frac{\partial U_i}{\partial x_j}-\frac{\partial U_j}{\partial x_i}\right)-\varepsilon_{ijk}\Omega_k \quad (7)$$

and Ω_k is the rotation rate of the coordinate system. The empirical coefficients in the quadratic relationship by Speziale[13] are given as

$$C_1=-0.1512, C_2=0.0, C_3=0.0 \quad (8)$$

A more complex version of the RANS turbulence model is a second-order closure model, which is the Reynolds stress model(RSM). It is based on exact transport equations for the individual Reynolds stresses derived from the Navier-Stokes equations based on the ε-equation, Eq. (2). The exact differential equation describing

the behavior of the Reynolds-stress tensor τ_{ij} for an incompressible fluid is

$$\frac{\partial \tau_{ij}}{\partial t} + U_k \frac{\partial \tau_{ij}}{\partial x_k} = -P_{ij} + \frac{2}{3}\rho\varepsilon\delta_{ij} - \phi_{ij} + C_s \frac{\partial}{\partial x_k}\left(\frac{k}{\varepsilon}\left(\tau_{im}\frac{\partial \tau_{jk}}{\partial x_m} + \tau_{jm}\frac{\partial \tau_{ik}}{\partial x_m} + \tau_{km}\frac{\partial \tau_{ij}}{\partial x_m}\right)\right). \quad (9)$$

The four terms on the right-hand side represent the production tensor, the dissipation tensor, the pressure-strain correlation tensor, and the turbulent-transport tensor, respectively. The production tensor P_{ij} is defined as

$$P_{ij} = \tau_{ik}\frac{\partial U_j}{\partial x_k} + \tau_{jk}\frac{\partial U_i}{\partial x_k}. \quad (10)$$

The pressure-strain correlation tensor ϕ_{ij} is the correlation for the slow pressure strain and the rapid pressure strain. It can be expressed as the following correlation.

$$\phi_{ij} = \phi_{ij1} + \phi_{ij2} \quad (11)$$

where

$$\phi_{ij1} = -\rho\varepsilon\left(C_{s1}a_{ij} + C_{s2}\left(a_{ik}a_{kj} - \frac{1}{3}a_{mn}a_{mn}\delta_{ij}\right)\right) \quad (12)$$

$$\phi_{ij2} = -C_{r1}P_{mn}a_{ij} + C_{r2}\rho k S_{ij} - C_{r3}\rho k S_{ij}\sqrt{a_{mn}a_{mn}} + C_{r4}\rho k\left(a_{ik}S_{jk} + a_{jk}S_{ik} - \frac{2}{3}a_{mn}S_{mn}\delta_{ij}\right) + C_{r5}\rho k\left(a_{ik}\Omega_{jk} + a_{jk}\Omega_{ik}\right) \quad (13)$$

and a_{ij} is the anisotropic tensor defined as

$$a_{ij} = \frac{\overline{u_i'u_j'}}{k} - \frac{2}{3}\delta_{ij} \quad (14)$$

The closure coefficients proposed by Launder-Reece-Rodi(LRR) and Speziale-Sarkar-Gatski(SSG) are respectively given as

$$C_s = 0.22, C_{\varepsilon 1} = 1.45, C_{\varepsilon 2} = 1.9, C_{s1} = 1.8, C_{s2} = 0.0, \quad C_{r1} = 0.0, C_{r2} = 0.8, C_{r3} = 0.0, C_{r4} = 0.873, C_{r5} = 0.655 \quad (15)$$

$$C_s = 0.22, C_{\varepsilon 1} = 1.45, C_{\varepsilon 2} = 1.9, C_{s1} = 1.7, C_{s2} = -1.05, \quad C_{r1} = 0.9, C_{r2} = 0.8, C_{r3} = 0.65, C_{r4} = 0.625, C_{r5} = 0.2 \quad (16)$$

3. Numerical Method

3.1. CFD Model and Boundary Condition

The present study simulated an experimental study of a turbulent air flow in a central subchannel of 37-rod heated bundles with a triangular array (Figure 2) at two different pitch-to-diameter ratios (P/D=1.06 and P/D=1.12), which was conducted by Krauss and Meyer[7]. The rod diameter is 140 mm and the axial length is 6.9 m. Only the 1/6 triangular central channel of the rod bundle was modeled using flow symmetry to reduce the size of the computational model. The symmetric boundary condition was applied at the side flow boundaries, including the centerline, diagonal, and rod-to-rod gap. No-slip and constant heat flux were set at the rod surface. A uniform flow was provided at the inlet boundary and a constant pressure at the exit boundary.

Body-fitted and non-staggered structured grid

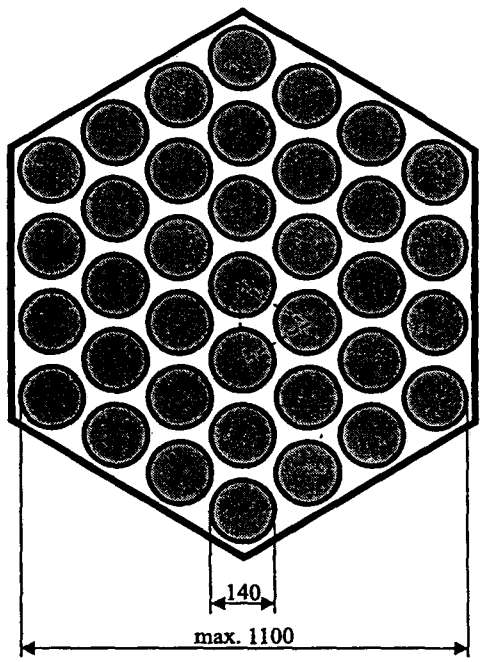

Fig. 2. A 37-rod Heated Bundle with a Triangular Array

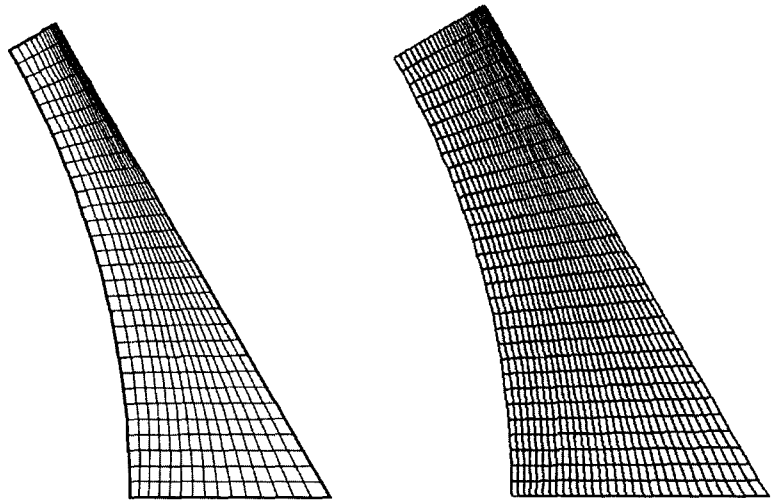

Fig. 3. Cross-sectional Meshes for a Central Subchannel of the Triangular Rod Array with a P/D=1.06 and P/D=1.12

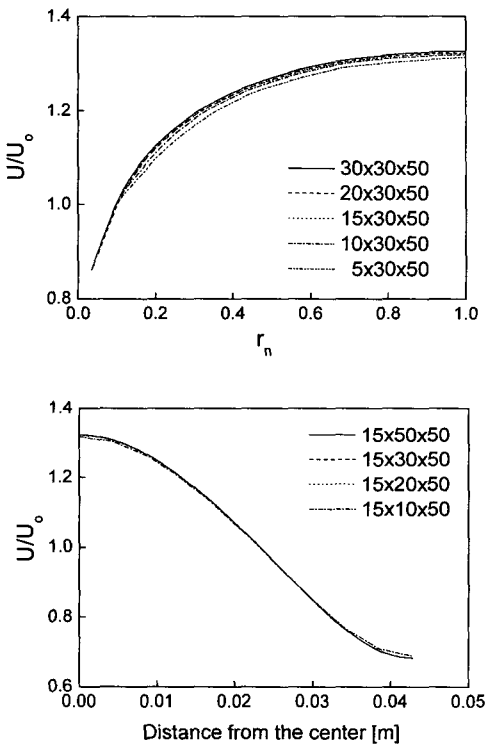

Fig. 4. Grid Test Results: the Effect of the Number of Radial and Azimuthal Nodes on the Distributions of Axial Velocity Along the Diagonal (top) and the Centerline (bottom)

systems were used to deal with the subchannel geometry. Figure 3 shows the cross-sectional meshes of the 1/6 central subchannel for P/D=1.06 and P/D=1.12. The optimal computational grids were found to be 15x30x50 for P/D=1.06 and 30x30x100 for P/D=1.12 in the radial, azimuthal, and axial directions, respectively. Figure 4 illustrates the effect of the number of radial and azimuthal nodes showing the optimal grid of 15x30x50 for P/D=1.06. The grid size in the non-dimensional wall unit (y^+) was calculated to be 35-70 and 30-37 for P/D=1.06 and P/D=1.12, respectively, which is the closest distance from the rod surface. The conventional wall functions using a universal law of the wall were applied to specify the turbulence in the near-wall region.

3.2. Numerical Procedure

This study used the commercial CFD codes, CFX-4.4[19] and CFX-5.6[20], to perform numerical experiments with various turbulence models. The nonlinear k-ε models were implemented in the commercial CFD code, CFX-

4.4[19] by direct modifications of the source routine, since they are not available in the CFX codes. The SIMPLEC algorithm is used to solve the velocity-pressure coupling. The SIMPLEC is a modification of SIMPLE, which differs in its derivation of the velocity correction equation. The linearised difference equation for the pressure-correction is solved by the algebraic multi-grid method. The second-order finite differencing scheme was used to discretise the convection term. Iterative calculation with a standard under-relaxation was used to obtain the converged solution. The calculation was terminated when the residual for the mass equation (sum of the absolute values of the net mass flux into or out of every cell in the flow field) was less than 0.001% of the total inlet mass flow rate and the residual reduction factors for the other governing equations were less than 10^{-4}.

The calculations were performed at Reynolds numbers, based on a bulk mean velocity(Uo) and hydraulic diameter of 39000 and 65000 for P/D=1.06 and P/D=1.12, respectively. The constant wall heat fluxes and the fluid temperature at the inlet were set at 0.98 kW/m2 and 5.8℃ for P/D=1.06, and 1.39 kW/m^2 and 12.3℃ for P/D=1.12, respectively.

4. Results and Discussions

The predicted distributions of the axial velocity in a central subchannel are compared with the measured ones in Figure 5. The standard $k-\varepsilon$ model shows the most rapid decrease of velocity from the center of the channel to the gap. The Speziale quadratic $k-\varepsilon$ model and the SSG-RSM

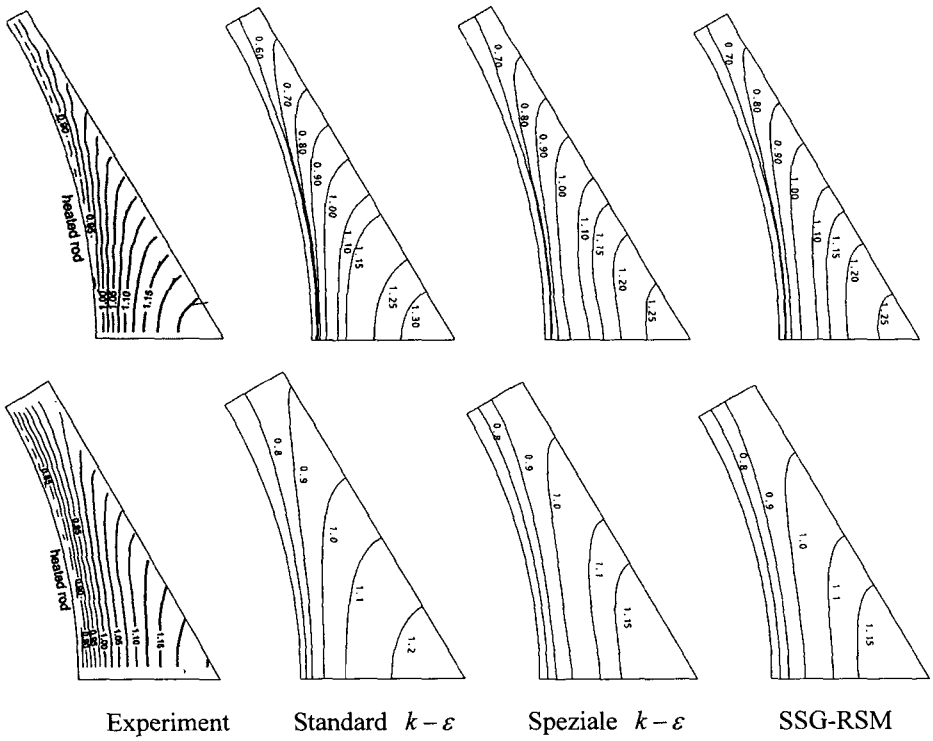

Fig. 5. Comparisons of the Velocity Distributions for P/D=1.06(top) and P/D=1.12(bottom)

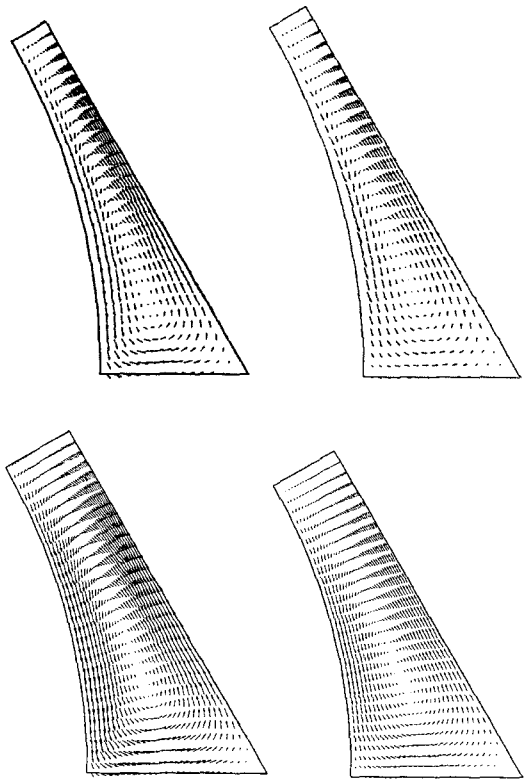

Fig. 6. Turbulence-driven Secondary Flow for P/D=1.06(top) and P/D=1.12(bottom)

predicted velocity distributions display an improved agreement with the measured ones. Similarly, for the measured velocity distributions, the Speziale model and SSG-RSM predicted velocity contours that were remarkably distorted for the gap region. The center-to-gap velocity ratio can be calculated as 2.0(Standard), 1.67(Speziale & SSG-RSM), and 1.33(Experiment) for P/D=1.06, and 1.36 (Standard), 1.28(Speziale & SSG-RSM), and 1.26(Experiment) for P/D=1.12, respectively. It is also noted that the LRR Reynolds stress model yielded nearly the same predictions as the SSG-RSM.

Figure 6 illustrates the turbulence-driven secondary flow predicted by the Speziale model and SSG-RSM. The secondary flow has been known to be formed by an anisotropic turbulence. Hence, the linear standard k-ε model could not predict the secondary flow because it is an isotropic model. The secondary flow, appears to occur in a symmetric pattern inside the subchannel, in the direction from the center to the gap along the centerline and turns back azimuthally along the rod surface. The maximum secondary velocity was estimated as 0.01Uo (Speziale) and 0.007Uo(SSG-RSM) for P/D=1.06, and 0.007Uo(Speziale) and 0.004Uo(SSG-RSM) for P/D=1.12, respectively. Therefore the magnitude of the secondary flow decreases as the pitch-to-diameter ratio increases.

Figure 7 compares the distributions of the fluid temperature, showing a larger variation in the predictions, i.e., a lower temperature in the central region and a higher one in the gap region, than the measured ones. The fluid temperature in the gap region is predicted to be even higher than the mean temperature of the rod surface($T_{w,m}$) for P/D=1.06. Thre is also a smaller variation of the fluid temperature for a larger pitch-to-diameter ratio, i.e., P/D=1.12. The difference between the prediction and the experiment decreases as the pitch-to-diameter ratio increases. The anisotropic turbulence models such as the Speziale k-ε model and the SSG-RSM predicted a more accurate temperature distribution than the standard k-ε model. The temperature contours by the Speziale model are more distorted for the gap region than the other predictions. This appears to be caused by a higher secondary flow to the gap by the prediction of Speziale model, as shown in Figure 6. Since the predictions by the LRR-RSM are almost the same as those by the SSG-RSM, they are not described separately.

The distributions of the wall shear stress along the rod surface are compared in Figure 8 against the experimental results. The Speziale k-ε model

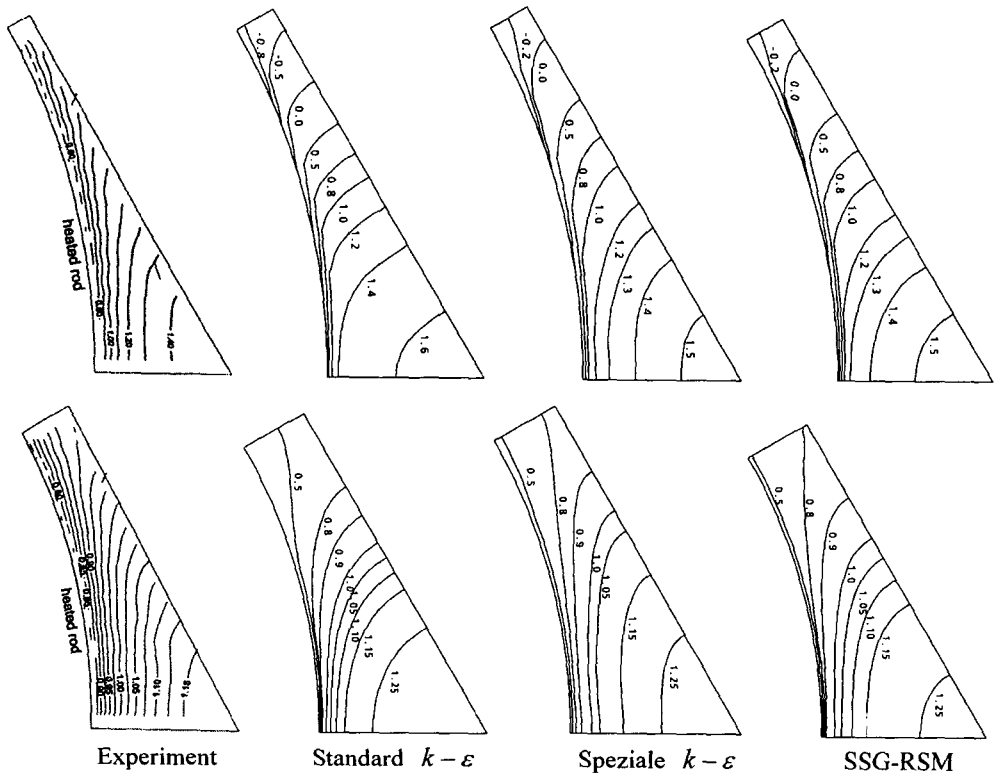

Fig. 7. Distributions of the Fluid Temperature ($(T_{w,m}-T)/(T_{w,m}-T_b)$) for P/D=1.06(top) and P/D=1.12(bottom)

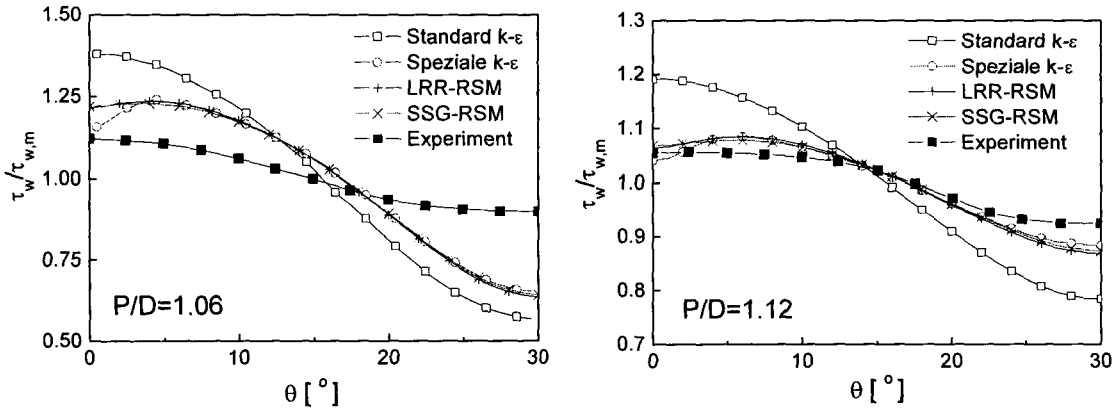

Fig. 8. Wall Shear Stress Distributions

and the RSM(SSG & LRR) gave significantly more accurate predictions than the standard model. However, the predictions show much large variation in the azimuthal direction than the measured ones. It can be seen that the discrepancy between the predictions and the measured ones becomes larger as the pitch-to-diameter ratio decreases. This indicates that

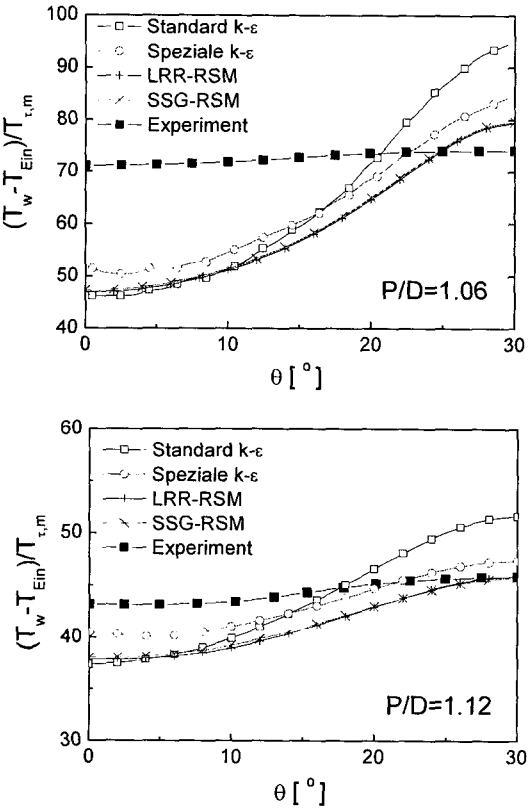

Fig. 9. Wall Temperature Distributions(T_{Ein} =5.8℃ for P/D=1.06, T_{Ein}=12.3℃ for P/D=1.12)

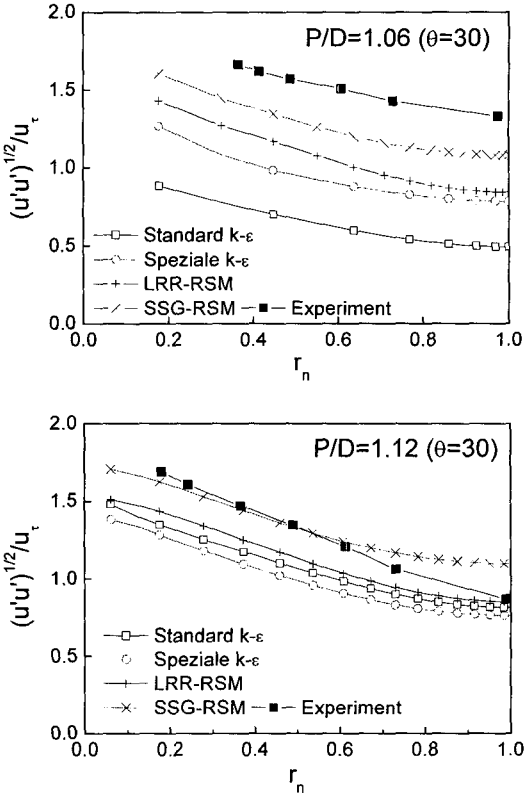

Fig. 10. Radial Profiles of the Axial Turbulence Intensity at the Gap

current turbulence models do not appropriately predict the unique turbulence structure (e.g., high turbulent mixing) in a very tight rod array. It is also noted that the anisotropic turbulence models, especially the Speziale model, tend to predict a peak value at about $\theta = 5$ near the diagonal of the subchannel. This is assumed to occur from secondary flow recirculating along the diagonal, as shown in Figure 6.

Figure 9 compares the wall temperature distributions along the rod surface. The wall temperatures were predicted to significantly vary along the rod surface in the azimuthal direction, i.e., a lower temperature near the diagonal(θ=0) and a higher temperature in the gap(θ=30). The discrepancy between the predictions and the measurements becomes larger as the pitch-to-diameter ratio decreases. Again, this is due to the inadeguacy of the current turbulence model when modeling a high turbulent mixing in a rod bundle. However, it can be concluded that the anisotropic turbulence models show better predictions than the isotropic standard k-ε model.

Figure 10 compares the radial profiles of the axial (streamwise) turbulence intensity at the gap of the rod bundle. Turbulence intensity for the standard k-ε is estimated from the turbulent kinetic energy, assuming isotropy. The profiles show a gradual decrease from the rod surface(r_n=0.0) to the center of the gap(r_n =1.0). The comparisons show under-predictions for P/D=1.06, but good predictions for P/D=1.12. It can be concluded

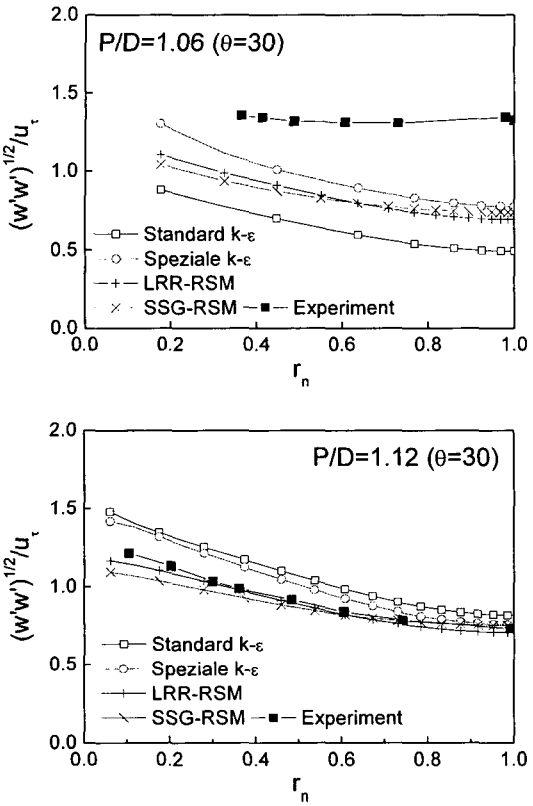

Fig. 11. Radial Profiles of the Azimuthal Turbulence Intensity at the Gap

that the SSG-RSM predicts the axial turbulence intensity closest to the measured values. The radial distributions of the azimuthal turbulence intensity at the gap are shown in Figure 11. The measured azimuthal intensity for P/D=1.06 is as high as the axial intensity in magnitude and is kept almost constant. The predictions for P/D=1.06 are significantly lower than the measured ones and decrease as it moves to the center of the gap. However, the predictions for P/D=1.12 agree reasonably well with the measured ones. The SSG-RSM predicts a higher axial intensity than the LRR-RSM, but the azimuthal intensity is similar to the LRR-RSM. It is also noted that the Speziale k-ε model predicts a lower axial intensity and a higher azimuthal intensity than the Reynolds stress models.

5. Conclusions

A numerical experiment using a CFD method analysis has been performed to investigate the turbulent flow and heat transfer in a triangular rod bundle with pitch-to-diameter ratios of 1.06 and 1.12. CFD predictions using various turbulence models were compared with the experimental results for the rod bundle and the conclusions can be summarized as follows;

1) The anisotropic turbulence models predicted the turbulence-driven secondary flow in the triangular subchannel and the distributions of the time mean velocity and temperature, showing a significantly improved agreement with measurements from the standard k-ε model.
2) The SSG Reynolds stress model predicted the turbulence intensities as well as the wall shear stress and the wall temperature which are the closest to the experiment results.
3) A large discrepancy between the CFD result and the experiment is observed for the rod bundle with a smaller pitch-to-diameter ratio.
4) A new turbulence model should be developed to more accurately predict the turbulence structure in a rod bundle.

Nomenclature

r_n	Normalized distance from the wall (dimensionless)
T	Fluid temperature (K)
T_b	Bulk mean fluid temperature (K)
T_{Ein}	Inlet temperature (K)
T_w	Wall temperature (K)
$T_{w,m}$	Mean wall temperature (K)
$T_{\tau,m}$	Mean friction temperature (K)

U Velocity of mean flow (m s^{-1})
u_τ Local friction velocity (m s^{-1})
u' Axial turbulence intensity (m s^{-1})
w' Azimuthal turbulence intensity (m s^{-1})

Greek

δ Kronecker delta
μ Dynamic viscosity (m^2 s^{-2})
ρ Fluid density (kg m^3)
σ Turbulent Prandtl number
τ_{ij} Reynolds stress tensor (N m^{-2})
$\tau_{W,m}$ Mean wall shear stress (N m^{-2})

Acknowledgment

The authors express their appreciation to the Ministry of Science and Technology of Korea for its financial support.

References

1. P. Carajilescov and N. E. Todreas, "Experimental and analytical study of axial turbulent flows in an interior subchannel of a bare rod bundle," *J. Heat Transf., Trans. ASME*, 262-268 (1976).
2. V. Vonka, "Measurement of secondary flow vortices in a rod bundle," *Nucl. Engng. and Des.*, **106**, 191-207 (1988).
3. D. S. Rowe, B. M. Johnson, and J. G. Knudsen, "Implications concerning rod bundle crossflow mixing based on measurements of turbulent flow structure," Int. J. Heat Mass Transf., **17**, 407-419 (1974).
4. R. Eichhorn, H. C. Kao, and S. Neti, "Measurements of shear stress in a square array rod bundle," *Nucl. Engng. and Des.*, **56**, 385-391 (1980).
5. J. D. Hooper and D. H. Wood, "Fully developed rod bundle flow over a large range of Reynolds number," Nucl. Engng. and Des., **83**, 31-46 (1984).
6. K. Rehme, "The structure of turbulence in rod bundles and the implications on natural mixing between the subchannels," *Int. J. Heat Mass Transf.*, **35**(2), 567-581 (1992).
7. T. Krauss and L. Meyer, "Experimental investigation of turbulent transport of momentum and energy in a heated rod bundle," *Nucl. Engng. and Des.*, **180**, 185-206 (1998).
8. W. Slagter, "Finite element solution of axial turbulent flow in a bare rod bundle using a one-equation turbulence model," *Nucl. Sci. Engng.*, **82**, 243-259 (1982).
9. K. B. Lee and H. C. Jang, "A numerical prediction on the turbulent flow in closely spaced bare rod arrays by a nonlinear k-e model," *Nucl. Engng. and Des.*, **172**, 351-357 (1997).
10. M. S. J. Lemos and M. Asato, "Simulation of axial flow in a bare rod bundle using a non-linear turbulence model with high and low Reynolds approximations," *10th International Conference on Nuclear Engineering*, Arlington, VA, USA, April 14-18 (2002).
11. W. K. In, D. S. Oh, and T. H. Chun, "Simulation of turbulent flow in rod bundles using eddy viscosity models and the Reynolds stress model," *The 10th Int'l. Topical Meeting on Nuclear Reactor Thermal Hydraulics(NURETH-10)*, Seoul, Korea, October 5-9 (2003).
12. W. K. In, T. H. Chun, H. K. Myong, and K. Ko, "CFD simulation of axial turbulent flow in a triangular rod bundle," *The 5th Asian Computational Fluid Dynamics, Busan, Korea*, October 27-30 (2003).
13. C. G. Speziale, "On Non-linear k-l and k-e models of Turbulence," *J. Fluid Mech.*, **178**, 459-475 (1987).
14. T. H. Shih, J. Zhu, and J. L. Lumley, "A realizable Reynolds stress algebraic equation

model," *NASA Tech. Memo* 105993 (1993).

15. T. J. Craft, B. E. Launder, and K. Sugar, "Development and application of a cubic eddy-viscosity model of turbulence," *Int. J. Heat and Fluid Flow*, **17**, 108-115 (1996).
16. B. E. Launder, G. J. Reece, and W. Rodi, "Progress in the development of a Reynolds stress turbulence model," *J. of Fluid Mech.*, **68**, 537-566 (1975).
17. B. E. Launder and D. B. Spalding, "The numerical computation of turbulent flows," *Computational Methods in Applied Mech. and Engng.*, **3**, 269-289 (1974).
18. C. G. Speziale, S. Sarkar, and T. B. Gatski, "Modelling the pressure-strain correlation of turbulence: an invariant dynamical systems approach," *J. Fluid Mechanics*, **277**, 245-272 (1991).
19. CFX Ltd., CFX-4.4: Solver, Oxfordshire, United Kingdom (2001).
20. CFX Ltd., CFX-5.6: Solver, Oxfordshire, United Kingdom (2003).